THE UNIVERSITY of EDINBURGH

Edinburgh Research Explorer

Functionally conserved non-coding regulators of cardiomyocyte proliferation and regeneration in mouse and human

Citation for published version:
Adamowicz-Brice, M, Morgan, C, Haubner, BJ, Noseda, M, Collins, MJ, Abreu Paiva, M, Srivastava, PK, Gellert, P, Razzaghi, B, O'Gara, P, Raina, P, Game, L, Bottolo, L, Schneider, MD, Harding, SE, Penninger, J & Aitman, T 2018, 'Functionally conserved non-coding regulators of cardiomyocyte proliferation and regeneration in mouse and human', *Circulation: Cardiovascular Genetics*, vol. 11, no. 2. https://doi.org/10.1161/CIRCGEN.117.001805

Digital Object Identifier (DOI):
10.1161/CIRCGEN.117.001805

Link:
Link to publication record in Edinburgh Research Explorer

Document Version:
Peer reviewed version

Published In:
Circulation: Cardiovascular Genetics

General rights
Copyright for the publications made accessible via the Edinburgh Research Explorer is retained by the author(s) and / or other copyright owners and it is a condition of accessing these publications that users recognise and abide by the legal requirements associated with these rights.

Take down policy
The University of Edinburgh has made every reasonable effort to ensure that Edinburgh Research Explorer content complies with UK legislation. If you believe that the public display of this file breaches copyright please contact openaccess@ed.ac.uk providing details, and we will remove access to the work immediately and investigate your claim.

OPEN ACCESS

Download date: 06. May. 2023

Functionally conserved non-coding regulators of cardiomyocyte proliferation and regeneration in mouse and human.

Adamowicz, Morgan, Haubner

Transcriptomic regulation of cardiac regeneration.

Martyna Adamowicz, PhD[2,9], Claire C. Morgan, PhD[2,5,9], Bernhard J. Haubner, MD, PhD[3,4,9], Michela Noseda, MD, PhD[2], Melissa J. Collins, PhD[5], Marta Abreu Paiva, PhD[2], Prashant K. Srivastava, PhD[5], Pascal Gellert, PhD[6], Bonnie Razzaghi, BSc[5], Peter O'Gara, BSc[2], Priyanka Raina, PhD[5], Laurence Game, PhD[7], Leonardo Bottolo, PhD[8], Michael D. Schneider, MD, PhD[2], Sian E. Harding, PhD[2], Josef Penninger, MD[3,10] and Timothy J. Aitman, MD, PhD[1,5,10,11]

[1]Centre for Genomic and Experimental Medicine, Institute of Genetics and Molecular Medicine, University of Edinburgh, Edinburgh, UK

[2]National Heart and Lung Institute, Faculty of Medicine, Imperial College, London, UK

[3]IMBA, Institute of Molecular Biotechnology of the Austrian Academy of Sciences, Vienna, Austria

[4]Department of Internal Medicine III, Medical University of Innsbruck, Austria

[5]Department of Medicine, Faculty of Medicine, Imperial College, London, UK

[6]Physiological Genomics and Medicine, MRC Clinical Sciences Centre, London, UK

[7]Genomics Core Laboratory, MRC Clinical Sciences Centre, London, UK

[8]Department of Mathematics, Faculty of Natural Sciences, Imperial College, London, UK

[9]co-first authors

[10]co-senior authors

[11]To whom correspondence should be addressed:

Timothy Aitman

Centre for Genomics and Experimental Medicine

MRC Institute of Genetics & Molecular Medicine

The University of Edinburgh

Western General Hospital

Crewe Road South

Edinburgh, EH4 2XU

Tel: +44 (0) 131 651 1041

Fax: +44 (0) 131 651 8800

Email: tim.aitman@ed.ac.uk

Word count: 6951

Journal Subject Terms

Basic, Translational, and Clinical Research

- Computational Biology
- Cell Biology/Structural Biology
- Mechnisms
- Myocardial Regeneration

Genetics

- Gene Expression and Regulation

Heart Failure and Cardiac Disease

- Myocardial Infarction

Abstract

Background

The adult mammalian heart has little regenerative capacity after myocardial infarction (MI) while neonatal mouse heart regenerates without scarring or dysfunction. However, the underlying pathways are poorly defined. We sought to derive insights into the pathways regulating neonatal development of the mouse heart and cardiac regeneration post-MI.

Methods and Results

Total RNA-seq of mouse heart through the first 10 days of postnatal life (referred to as P3, P5, P10) revealed a previously unobserved transition in microRNA expression between P3 and P5 associated specifically with altered expression of protein-coding genes on the focal adhesion pathway and cessation of cardiomyocyte cell division. We found profound changes in the coding and non-coding transcriptome after neonatal MI, with evidence of essentially complete healing by P10. Over two thirds of each of the mRNAs, lncRNAs and microRNAs that were differentially expressed in the post-MI heart were differentially expressed during normal postnatal development, suggesting a common regulatory pathway for normal cardiac development and post-MI cardiac regeneration. We selected exemplars of miRNAs implicated in our data set as regulators of cardiomyocyte proliferation. Several of these showed evidence of a functional influence on mouse cardiomyocyte cell division. In addition, a subset of these microRNAs, miR-144-3p, miR-195a-5p, miR-451a and miR-6240 showed evidence of functional conservation in human cardiomyocytes.

Conclusions

The sets of mRNAs, miRNAs and lncRNAs that we report here merit further investigation as gatekeepers of cell division in the postnatal heart and as targets for extension of the period of cardiac regeneration beyond the neonatal period.

Key words: myocardial infarction, coding and non-coding RNA, transfection, cardiomyocyte, miRNA

Background

Heart disease is amongst the commonest causes of death worldwide[1]. Whilst planarians, teleost fish and some amphibians have the ability to regrow limbs or organs including the heart[2-4], mammals are limited in their regenerative abilities[5,6]. Following myocardial infarction (MI), damaged myocardium is replaced by scar tissue triggering cardiac remodelling and impaired cardiac function[7,8].

A major barrier to cardiac regeneration in adult mammals is the withdrawal of the cardiomyocyte from the cell cycle in early postnatal life. In the mouse, although DNA replication continues in the first week of postnatal life, cytokinesis ceases. By the second week of life, mouse cardiomyocytes withdraw from the cell cycle, 90% of cardiomyocytes are binucleated and, aside from a recent report of a proliferative burst at P15[9], recently contested[10], heart growth after the first week of life occurs mainly through cardiomyocyte hypertrophy rather than proliferation[11,12]. This programme of cell cycle arrest is hypothesised to result from metabolic, physiological and anatomical changes in the first week of life including a shift to oxidative metabolism with relative hyperoxia compared to foetal life, increasing ventricular pressure and accumulation of extracellular matrix[13]. These considerations raised the possibility that regeneration of the mouse heart could follow cardiac injury in the immediate neonatal period and indeed complete cardiac regeneration has recently been demonstrated following apex resection and infarction of the mouse left ventricle (LV) on the first day of postnatal life[14-16].

Transcriptome analyses in planarians and amphibians have yielded significant insights into the regulatory mechanisms underlying tissue and organ regeneration in these species[17-19] but morphological, physiological and genetic differences between these species and mammals

limit the translational potential for application to human disease. They do, however provide the basis of the molecular investigations in mammals[19]. In mice, the role of individual microRNAs (miRNAs) and protein-coding messenger RNAs (mRNAs) have been defined by genetic analyses and gene targeting of specified mRNAs and miRNAs[16,20,21]. More recently with recognition of the functions of other RNA species, certain long non-coding RNAs (lncRNAs) have been implicated in cardiac biology[22], for example, in protection from cardiac hypertrophy, foetal heart development, and autophagic cell death in myocardial infarction[23-26]. Although previous genome-wide studies have examined the coding transcriptome in neonatal and regenerating heart following apical resection[27], genome-wide changes in the non-coding transcriptome have not been reported.

Here we have performed an in-depth analysis of the coding and non-coding mouse LV transcriptome by RNA sequencing at key time points in early postnatal mouse heart development and in the LV during the period of regeneration following neonatal ligation of the left anterior descending coronary artery (LAD). The study defines the major sets of coding and non-coding RNAs associated with normal postnatal cardiac development and with regeneration of the neonatal heart following MI. We perform functional studies on a key set of exemplar miRNAs in mouse and human cardiomyocytes and identify conserved roles for these miRNAs in mammalian cardiomyocyte proliferation and mitosis. Our study provides new insights into the transcriptional regulation of neonatal cardiac development and regeneration in mammals that will be of value in future comparative and human intervention studies of cardiac regeneration.

Materials and Methods

The data, analytic methods, and study materials have been made available to other researchers for purposes of reproducing the results or replicating the procedure. They have been made publicly available at the Annotare, accession number E-MTAB-6272. All animal experiments

were performed in accordance with the Austrian Ethical Board, the Imperial College and the UK Home Office guidelines.

Left anterior descending artery (LAD) ligation was performed in P0.5 neonatal C57BL6J mice, as previously described [15]. Left ventricle (LV) was harvested from three C57BL6J mice from sham-operated and LAD-ligated animals at three, five, seven and 10-days post ligation. Left ventricle (LV) was also harvested from three C57BL6J mice at P1, P3, P5, P7, P10 (referred to as physiological time points) in which no surgical procedures had been performed. Coding and non-coding RNA-Seq libraries were prepared using Illumina TruSeq stranded RNA library preparation and TruSeq small RNA library preparation kits following manufacturers' protocols. Mouse genome assembly GCRm38/mm10 and the Ensembl transcript annotations (version GRCm38.87) were used as the reference sequence in all the analyses. RNA-Seq reads were quantified using Salmon (v.0.8.2)[28]. Differential expression (DE) analysis was performed using DESeq2 Bioconductor package. Raw p values were adjusted for multiple testing with the Benjamini-Hochberg procedure. Weighted gene co-expression cluster analysis (WGCNA) and a short timer series expression miner (STEM) analysis were performed to identify clusters of co-expressed mRNAs. Enrichment of KEGG Pathways for DE mRNAs was calculated using DAVID (v6.8) across all pairwise comparisons. MiRNA-Seq reads were aligned with Bowtie and MirDeep2 was used to determine the presence and quantity of miRNAs based on mouse precursor sequences and mature sequences from mouse and rat with miRBase release 19. MiRNA binding sites were predicted in-silico across each gene using the union of five separate prediction methods. Correlation matrices were generated between mRNAs and miRNAs and between mRNAs and lncRNAs. Potential functional relationships were identified by Spearman correlation, adjusted for multiple testing correction at FDR < 0.05. P5 mouse cardiomyocytes were treated with mmu-miR-22-5p, mmu-miR-144, mmu-miR-148a-3p, mmu-miR-193a-3p, mmu-miR-193b-3p, mmu-miR-221-3p, mmu-miR-331-3p, mmu-miR-451a inhibitors and

mmu-miR-6240 mimic and iCell® Cardiomyocytes were treated with human analogues of these miRs. Cells were incubated 10 μM EdU 4 h after seeding and subsequently fixed with 4% paraformaldehyde and permeabilized in 0.2% (v/v) Triton X-100 before incubation with Click-iT reaction. Hoechst was used for nuclear staining and pH3 to mark mitotic cells. The analysis was then performed with conventional epifluorescence microscopy.

Results

To define the transcriptional changes occurring during physiological postnatal cardiac development and after neonatal MI, we generated RNA-Seq expression data of the coding and non-coding transcriptome from triplicate LV tissue harvested from C57BL/6 mice on postnatal day 0.5, 3.5, 5.5, 7.5 and 10.5, referred to as P1, P3, P5, P7 and P10, and from LV at 3 to 10 days following LAD ligation (Figure 1).

Transcriptional changes in coding RNA

During the time course of physiological postnatal growth from P1 to P10, we identified 9,450 unique differentially expressed (DE) mRNAs across all possible pairwise comparisons (Supplemental Table 1).

We identified an increase in gene expression of 11 cardiomyocyte markers at different time points and an increase in cardiac fibroblast marker (*Ddr2*) after P5, reflecting the change in cellular composition within the LV (Supplemental Figure 1). WGCNA and STEM analyses of these genes identified clusters enriched for focal adhesion (p-adj = 1.22E-13), DNA replication (5.47E-16), ribosome (1.64E-50) and OXPHOS (p-adj = 0.013) pathways of KEGG analysis (Supplemental Figure 2A, B). These results were affirmed in pairwise comparisons between time points, with enrichment for DNA replication genes between P1 and P5, oxidative phosphorylation, focal adhesion genes between P3 and P10, and ribosomal transcripts throughout a 10-day period (Figure 2A, Supplemental Table 2). Investigation of pairwise comparisons between adjacent time points revealed a sharp increase in the number of

differentially expressed genes (DEG) from between P3 to P5 (494) to P5 to P7 (3,545), with the largest number identified between P7 and P10 (4,375) (Figure 2B, Supplemental Figure 3A). Of the 40 most DEG between P5 and P7, 10 genes (*Ube2c, Kif20a, Top2a, Racgap1, Cdca3, Cenpf, Ccna2, Iqgap3, Anln, Ccnb1 and CenpE)* had GO terms associated with mitotic cell cycle process all of which were downregulated between P5 and P7 (Figure 2C, Supplemental Figure 2B).

Following sham operation and LAD ligation, transcriptome analysis showed a large number of DEG between sham-operated and LAD-ligated mice three days after injury (shamvLAD (P3) = 2,741). The number of DEG declined very sharply three days post ligation, with 499 genes found to be DE between sham and LAD at P5, 112 between sham and LAD at P7, and 61 between sham and LAD-ligated at P10 (Figure 2D, Supplemental Figure 3B). Upregulation of sarcomere expressed *Mypn* and cardiac fibroblast marker *Ddr2* was observed following LAD ligation at P3 with restoration of physiological expression profile of cardiomyocyte markers from P7 (Supplemental Figure 1B).

STEM analysis of the post-LAD ligation data showed 15 statistically significant profiles of changing gene expression, which had generally decreasing gene expression related to immune processes such as phagosome (p-adj = 5.9E-9) and cytokine-cytokine receptor interaction (p-adj=8.77E-8) (Supplemental Figure 2C). Four profiles (40, 42, 48 and 49) showed increasing gene expression pattern and were significantly enriched for OXPHOS which was also observed in the WGCNA analysis (Supplemental Figure 2C, D). STEM analysis of mRNA expression in the sham-operated mice (P3-P10) showed pathway enrichment for 13 profiles, mirroring enrichments observed in the physiological samples.

Consistent with the STEM annotation analysis, pairwise comparisons of the sham and LAD data at P3 showed that the major classes of DEG between P3 sham and LAD were within OXPHOS and lysosome pathways (Figure 2E, Supplementary Table 4). Of the top 40 most

significant DE mRNAs, we identified five genes (*Fn1*, *Col1a1*, *Tnc*, *Thbs1* and *Col1a2*) with an increase in expression between sham and LAD at P3 that are implicated in focal adhesion pathways and three genes (*Cd68*, *Laptm5* and *Atp6v0d2*) representing lysosome pathways (Figure 2E, F). Strikingly, 74% of the 3,210 genes that were DE between sham and LAD were also DE in the pairwise comparisons in the normal physiological data (Figure 2G). Of the 10,284 DEG, 20 were validated and further characterised by qPCR across all conditions used in the study using an independent set of triplicate samples (Supplementary Figure 4A).

Changes in non-coding RNA transcriptome

Next, we analysed changes in the expression of non-coding RNAs including lncRNAs and miRNAs in the normal developing heart. Between all pairwise time point comparisons from P1 to P10, we identified 545 unique DE lncRNAs (Supplementary Table 1). A fourfold increase in the number of DE lncRNAs was observed between P3 and P5 (n=24) and between P5 and P7 (n=107) comparisons (Figure 3A). Only 59 of 545 DE lncRNAs have assigned names, for the remainder, there has been limited, functional characterisation. Four DE lncRNAs between P5vP7, within the top 40 DE, that have names and functions associated with them include: *Nespas, Sorbs2os, H19 and Lockd* (Figure 3B, Supplementary Table 1). This is the first report showing DE of any of these lncRNAs in the postnatal mammalian heart.

To explore potential interactions between lncRNAs and mRNAs in the developing heart, we tested for correlation between lncRNA and mRNA expression across P1 to P10 time points. Of the 545 DE lncRNAs, 491 correlated significantly ($p\text{-}adj_{Spearman} < 0.05$) with between 1 and 2,604 mRNAs either in *cis* or *trans*. Overall, we found that there were slightly more (median = 26) lncRNAs significantly correlating in *trans* compared to in *cis* (median = 15), implying that their regulatory potential is not limited by chromosomal location (Figure 3C).

To determine possible functional regulatory roles of DE lncRNAs, we performed a KEGG analysis on the sets of genes correlating in *cis* or *trans* with DE lncRNAs. We identified 86

lncRNAs that correlated significantly with gene sets enriched for the ribosome pathway, 113 for oxidative phosphorylation, and 103 with enrichment for the focal adhesion pathway (Supplementary Table 3).

Between sham-operated and LAD-ligated LV at P3 we identified 51 DE lncRNAs, 55 DE lncRNA at P5 and eight DE lncRNAs at P7. No DE lncRNAs were identified at P10 (Figure 3E, Supplementary Table 1), in keeping with the marked reduction in DE mRNAs and miRNAs at later time points. The 51 DE lncRNAs between sham and LAD comparisons at P3 include the known lncRNAs *H19*, *Dnm3os*, *Lockd*, *Malat1*, *Meg3*, *Mhrt*, *Mirt1*, *Neat1*, *Slmapos2*, *Zfp469* and 41 lncRNAs with unknown function (Figure 3E). A selection of these lncRNAs was significantly correlated with gene sets enriched in ribosome, OXPHOS, focal adhesion, lysosome and phagosome KEGG pathways (Supplementary Table 3). Seventy three of the 109 DE lncRNAs (67%) between sham and LAD were also DE between time points in the physiological samples (Figure 3F, Supplementary Table 3).

Analysis of small RNAs identified 413 DE miRNAs across all pairwise comparisons of physiological time points (Supplementary Table 4). Expression of 22 of 413 DE miRNAs was tested in separate samples from different animals, in all time points by qPCR and these were all validated (Supplementary Figure 4B). The changes were also validated in sorted cells' subpopulations, showing that the change of expression occurred both in cardiomyocytes and endothelial cells (data not shown). Of the 413 DE miRNAs, 240 were DE between the P3vP5 time points, 197 were unique (Figure 4A, Supplementary Table 4). The marked transition in expression of these miRNAs, between P3 and P5, has not previously been observed.

To identify the potential roles of DE miRNAs during the P1 to P10 time period, we examined the correlation between the 413 miRNAs that were DE between all the time points and all mRNAs expressed in these samples, and intersected these data with the *in silico* predicted binding partners of the DE miRNAs to give a set of RNAs that correlate with and may be

targeted by these miRNAs (Supplementary Figure 5). We identified 65 unique miRNAs where their significantly correlated gene targets are enriched for specific KEGG pathways, 34 of which target a total of 67 genes associated with the focal adhesion pathway (Supplementary Table 5). Interestingly, orthologues of 49 of these 65 miRNAs were also identified in the human genome and these showed conservation of gene targets for a median of 84% of the orthologous genes within the human pathways (Supplementary Table 5).

We also investigated the temporal relationship between miRNAs and mRNAs. The 240 DE miRNAs, identified between P3 and P5, are predicted to target 2,731 mRNAs. Of these mRNAs, we observed a significant overlap with 222 of 494 of DE mRNAs between P3 and P5 (OR=2.09, p=7.51e-15) and 1,091 of the 3,545 DE mRNAs between P5 and P7 (OR=1.18, p=3.79e-4).

Small RNA-seq analysis showed 153 DE miRNAs between sham and LAD three days post ligation, followed by a marked decline in the number of DE miRNAs between sham and LAD at later time points (Figure 4D). The top 40 significantly DE miRNAs between sham and LAD at P3 have not been previously reported as DE following LAD ligation (Figure 4E). The 153 DE miRNAs identified between sham and LAD at P3 are predicted to target 2,231 mRNAs. Of these 2,231 mRNAs, 1,090 overlap with the 2,741 DE mRNAs identified between sham and LAD at P3 (OR=2.06, p<2.2e-16).

Of the 39 DE miRNAs that correlated with and have predicted targets amongst the DE mRNAs, 14 miRNAs target gene sets of between 9 and 314 genes in pathways for cancer, and 14 miRNAs target between 13 and 23 mRNAs in focal adhesion (Figure 4E, Supplementary Table 5). Interestingly, 31 of 39 miRNAs were conserved in humans and targeted a median of 75.7% of the orthologous genes in corresponding human pathways. Mirroring the mRNA data, 83% of the miRNAs that were DE between sham and LAD were also DE in the pairwise comparisons between the physiological time points (Figure 4F).

Functional analysis of miR inhibition and overexpression in P5 mouse cardiomyocytes

To test the functional effects of miRNAs on cardiomyocyte proliferation we performed inhibition and overexpression studies in mouse and human cardiomyocytes, on a set of miRNAs that exhibited significant changes in physiological and pathological conditions and correlated with changes in mRNA in focal adhesion pathway We obtained over 80% reduction of the expression of nine miRNAs in primary mouse cardiomyocytes and a subset of four of their human orthologues in iCell® cardiomyocytes, and over 50% overexpression of miR-6240 (data not shown). qRT-PCR analysis of the expression of cell cycle-regulating cyclins revealed that the levels of *Ccna2*, *CcnD2* and *CcnE2* increased significantly (> 2-fold) following treatment with miR-22-5p, miR-451a and miR-195a inhibitors, and with miR-6240 mimic, in comparison to cells treated with scramble ($p < 0.05$) (Figure 5A). Treatment with seven other miR inhibitors did not result in any significant changes ($p > 0.05$) of tested cyclins expression (Figure 5A). Expression of *Ccna1*, *CcnD1*, *CcnD3* and *CcnE1* did not change in response to inhibition or overexpression of any of the miRNAs.

To determine whether inhibition or overexpression of these miRs plays a direct role in promoting cardiomyocyte proliferation we measured the nuclear incorporation of EdU (S-phase marker) and pH3 staining (mitosis marker) in P5 mouse cardiomyocytes. A marked increase in proliferating (EdU positive) cells (up to 5-fold) was observed for cardiomyocytes treated with miR-22-5p, miR-144-3p, miR-148a-3p, miR-193a-3p, miR-193b-3p, miR-195a-5p, miR-221-3p, miR-331-3p, miR-451a inhibitors and miR-6240 mimic (Figure 5B). Likewise, an increase of mitotic (pH3 positive) cells was seen (up to 3-fold), following treatment with miR-22-5p, miR-195a-5p and miR-451a inhibitors and miR-6240 mimic (Figure 5C, Supplementary Figure 6A). Scramble-treated mouse cells served as the negative control for both assays.

Functional analysis of selected miRs in human cardiomyocytes

Given our data showing that several miRNAs regulate aspects of proliferation in P5 mouse cardiomyocytes, we tested whether the human orthologues of these miRNAs can functionally regulate cardiomyocyte proliferation in iCell® cardiomyocytes. We transfected iCell® cardiomyocytes with a subset of human miR inhibitor and mimic orthologues that we had previously tested in mouse cardiomyocytes. qRT-PCR analysis of cyclins expression revealed elevated levels of *Ccna2*, *CcnD2* and *CcnE2* in miR-22-5p, miR-451a and miR-6240 treated cells in comparison with scramble treatment ($p < 0.05$) (Figure 5D). As with the mouse miR interventions, levels of *Ccna1*, *CcnD1*, *CcnD3* and *CcnE1* were unchanged (Figure 5D). iCell® cardiomyocytes treatment with miR-6240 mimic showed an increase in number of proliferating cells and treatment with miR-144-3p, miR-195a-5p, miR-451a and miR-6240 showed up to a 2–fold increase in the number of mitotic cells (Figure 5E, F, Supplementary Figure 6B).

Discussion

We set out to define the programme of the coding and non-coding transcriptome in the healthy neonatal heart during the period of loss of regenerative capacity and to relate this to the transcriptional changes associated with cardiac regeneration following neonatal MI. We found a sharp transition in microRNA expression in the developing heart between P3 and P5 associated with subsequent changes in expression of genes on the focal adhesion pathway and cardiomyocyte division arrest. We mapped profound changes in the transcriptome that returned to normal within 10 days following neonatal MI, indicating essentially complete healing of the myocardium by this time point, confirming our previous findings[15]. We showed that two thirds of all RNA species that were DE in the post-MI heart were also DE during normal postnatal development, suggesting a common regulatory pathway for normal post-natal cardiac development and post-MI regeneration. Finally, we demonstrated that miR-144-3p, miR-195a-5p and miR-451a inhibition and miR-6240 activation have functionally conserved roles in cell proliferation and mitosis in mouse and human cardiomyocytes.

We found that the first 10 days of postnatal life were associated with alterations in gene expression of thousands of genes, particularly those encoding proteins involved in cell cycle progression at early time points, oxidative phosphorylation at later time points and protein translation throughout. These enriched pathways are likely reflective of changes in ventricular pressure, transition from hypoxic to the oxygen rich postnatal environment with increased reliance on oxidative metabolism, and changes in cellular architecture and the extracellular matrix between P3 and P7[13,29]. During the P5 and P7 time window, one quarter of the most DEG correspond to GO terms associated with M-phase mitosis and mitotic cell cycle checkpoint, including *Cdk1*[30], *Ccna2*[31], *Cdc13*[32] and *Bub1*[33], in keeping with the withdrawal of cardiomyocytes from DNA replication and cell division at this time point. While the relative abundance of myocytes, cardiac fibroblasts, endothelial cells and vascular smooth muscle cells change in the LV during the first ten postnatal days[34] and ontologies and pathways identified through our transcriptomic study are in part reflective of this, we were able to identify putative drivers of cardiomyocyte proliferation and functionally validate them in mouse primary cells and human cardiomyocyte cell line.

We found major differences in mRNA, miRNA and lncRNA expression between LAD-ligated and sham-operated mice three days following MI, but these differences had almost completely resolved within seven days of LAD ligation and increased gene expression of cardiomyocyte markers is restored to mirror closely the physiological gene expression changes. At the transcriptional level, therefore, the regenerative process was essentially complete by P10, although certain developmental and cardiac failure markers, like *Nppa*[35], remained elevated. The most profoundly DEG three days post LAD were those involved in immune processes, similarly shown in the contrasting model of heart regeneration following apex removal together with cell cycle progression and RNA synthesis[27] and oxidative phosphorylation, in keeping

with previous observations of the importance of an active immune response in physiological regulation of cardiac regeneration in mice[36,37].

Similar changes in expression were observed with lncRNAs, where of the 107 DE lncRNAs between P5 and P7, only seven, including *H19* and *Neat1*, have proposed functions, in cell proliferation[38-40], and none have been previously associated with postnatal heart development or regeneration. We also found evidence for *trans*-regulation of expression by lncRNAs with enrichment amongst correlating gene sets on OXPHOS, ribosomes and focal adhesion pathways, and show significant enrichment for imprinting amongst DE lncRNAs. While previously described in other tissues[41], enrichment for imprinted loci has rarely been observed previously in the postnatal heart or following MI[42].

We observed a profound shift in microRNA expression in the developing heart between P3 and P5 associated with an altered expression of genes on the focal adhesion pathway between P5 and P7. Since genes and proteins on the focal adhesion pathway mediate the transduction of external stimuli such as increasing blood pressure or hypoxia[29,43 44] into processes such as DNA replication and cell division[45], we hypothesise that the set of miRNAs that were DE in the P3 to P5 time window are key to the regulation of molecular events leading to withdrawal of the cardiomyocyte from cell division in the first week of life. To test this hypothesis, we performed *in vitro* inhibition and over-expression studies on 10 miRNAs which exhibited significant changes in physiological and pathological conditions. They include two miRNAs (miR-195a-5p and miR-22-5p) for which previous evidence has been presented[20,46]. Our results demonstrate that the inhibition of miR-22-5p and miR-451a and miR-6240 up-regulation individually elevate the expression of *CcnA2*, *CcnD2* and *CcnE2* in P5 mouse and human cardiomyocytes leading to increased proliferation and cell division. We did not observe changes in expression of *CcnA1* (expressed in germ cells), *CcnE1* (lowly expressed in heart), *CcnD1* or *CcnD3* (low expression in tested cardiomyocytes) in comparison to scramble-treated

cells. Targets of miR-22 include *Map2k1*, *Map3k9*, *Rock2* representing the focal adhesion pathway, regulation of cell proliferation, and *Aurkb* participating in the regulation of alignment and segregation of chromosomes during cell division[47]. miR-451a targets *Tbx1* and *Ybx1* transcription factors regulating proliferation and differentiation of multipotent heart progenitors[48] and is implicated in translational control of foetal myocardial gene expression after cardiac transplant[49]. There is limited knowledge on the functional role of miR-6240, and here we show for the first time, its function in cardiomyocyte proliferation and heart regeneration in mouse and human cardiomyocytes[50]. Interestingly, miR-22 has been previously found to be highly expressed in cardiac muscle, upregulated during myocyte differentiation which alone has been found to be sufficient to induce cardiomyocyte hypertrophy.

Our study reports the transcriptional changes in the developing and post-MI postnatal heart and defines sets of mRNAs, miRNAs and lncRNAs that we propose to be the key regulators, at the level of the transcriptome, of withdrawal of the postnatal mouse heart from DNA replication and cell division. We also identify miR-144-3p, miR-195a, miR-451a and miR-6240 as functionally conserved, non-coding regulators of cardiomyocyte division in neonatal mouse and humans. Whilst we have not studied all the downstream consequences of our findings, including more detailed impact on protein, cell cycle, and *in vivo* validation, our work provides a platform for future studies.

Recent progress in research in developmental cardiology has significantly advanced our understanding of heart development and regeneration[51]. Insights from zebrafish models of heart regeneration, following apex removal or cryosurgery, show that they are capable of myocardial regeneration mediated mainly through the proliferation of pre-existing gata4^{+} cardiomyocytes with miR-133[52] and miR-101[53], playing regulatory roles in this process, as also shown in our neonatal mouse data set. More recently, the attempt to pinpoint the regulatory hubs in zebrafish heart regeneration revealed a function of i*l6st*, *adam8*, and *cd63* [19], also shown to be DE

394 expressed in our post-ligation data sets. Studies of heart regeneration in neonatal mice reported
395 *Myh7* and *Igf1r* as key drivers of gene interaction networks and pointing to *C1orf61*, *Aif1*,
396 *Rock1* as potential inhibitors of cardiomyocyte proliferation and G1/S phase transition[54], genes
397 that were also DE between physiological time points in our set. In addition, miRNAs from the
398 miR-15 family[20], miR-503-5p[54], miR-199a[55], miR-99/100 and Let7a/c[21] were also reported as
399 critical regulators of the regeneration process, which were also found as DE in our
400 physiological and sham/LAD comparisions in our data set. Interleukin 13, DE in the
401 regenerating neonatal heart in our data set, has also been identified as a regulator of
402 cardiomyocyte cell cycle entry mediated by STAT3/periostin and STAT6[27]. Whilst our data
403 show considerable overlap with previous observations in mice and zebrafish, we provide a
404 systematic and comprehensive analysis of coding and non-coding transcriptome changes over
405 multiple time points of the first 10 days of postnatal life and after neonatal LAD ligation, which
406 has not been available hitherto.
407 In summary, we present a finely grained time course for mRNA, miRNA and lncRNA in the
408 normal developing heart from postnatal day 1 (P1) to P10, and in the 3 to 10 days following
409 neonatal MI. We found profound changes in the coding and non-coding transcriptome after
410 neonatal MI, with evidence of essentially complete transcriptional healing by P10. We find a
411 sharp transition in miRNA expression in physiological cardiac samples between P3 and P5,
412 with differentially expressed miRNAs associated specifically with altered expression of genes
413 on the focal adhesion pathway and cessation of cardiomyocyte division. Two thirds of each of
414 the mRNAs, lncRNAs and microRNAs that were differentially expressed in the post-MI heart
415 were also differentially expressed during normal postnatal development, suggesting a common
416 regulatory pathway for normal cardiac development and post-MI cardiac regeneration. Of the
417 miRNAs that we implicate in regulation of cardiomyocyte development and regeneration, 67%
418 had targets that were conserved between mice and humans. We present a subset of miRNAs:

miR-451a, miR-6240, miR-195a-5p and miR-144-3p that showed functional evidence *in vitro* as regulators of cell division in mouse and/or human cardiomyocytes.

Acknowledgements

We thank the Leducq Foundation, the British Heart Foundation, the MRC CSC and Österreichischen Herzfonds for funding. We thank Imperial College High Performance Computing Service (http://www.imperial.ac.uk/admin-services/ict/self-service/research-support/hpc/) and IMP-IMBA Biooptics service facility for assistance in cell sorting. We gratefully thank David Porteous, Nicholas Hastie, Stuart Cook and Andrew Jackson for critical comments on the manuscript.

Sources of Funding

Leducq Foundation funding via the Transatlantic Network of Excellence (Grant 11CVD01), the British Heart Foundation funding via the Imperial College Centre of Research Excellence and the Imperial Cardiovascular Regenerative Medicine Centre RM/13/1/30157 and Österreichischen Herzfonds.

Disclosures

None

Accession Number

Reads are deposited in Annotare under accession code E-MTAB-6272.

Figure legends

Figure1. Experimental design.

Overview of experimental design showing time points at which LV tissue was harvested (A) during physiological time points, and following LAD or sham operation. P1-10, postnatal days 1-10; MI myocardial infarction, (B) sequencing pipeline and (C) functional investigation. All the experiments were performed in three individual animals for each time point and condition.

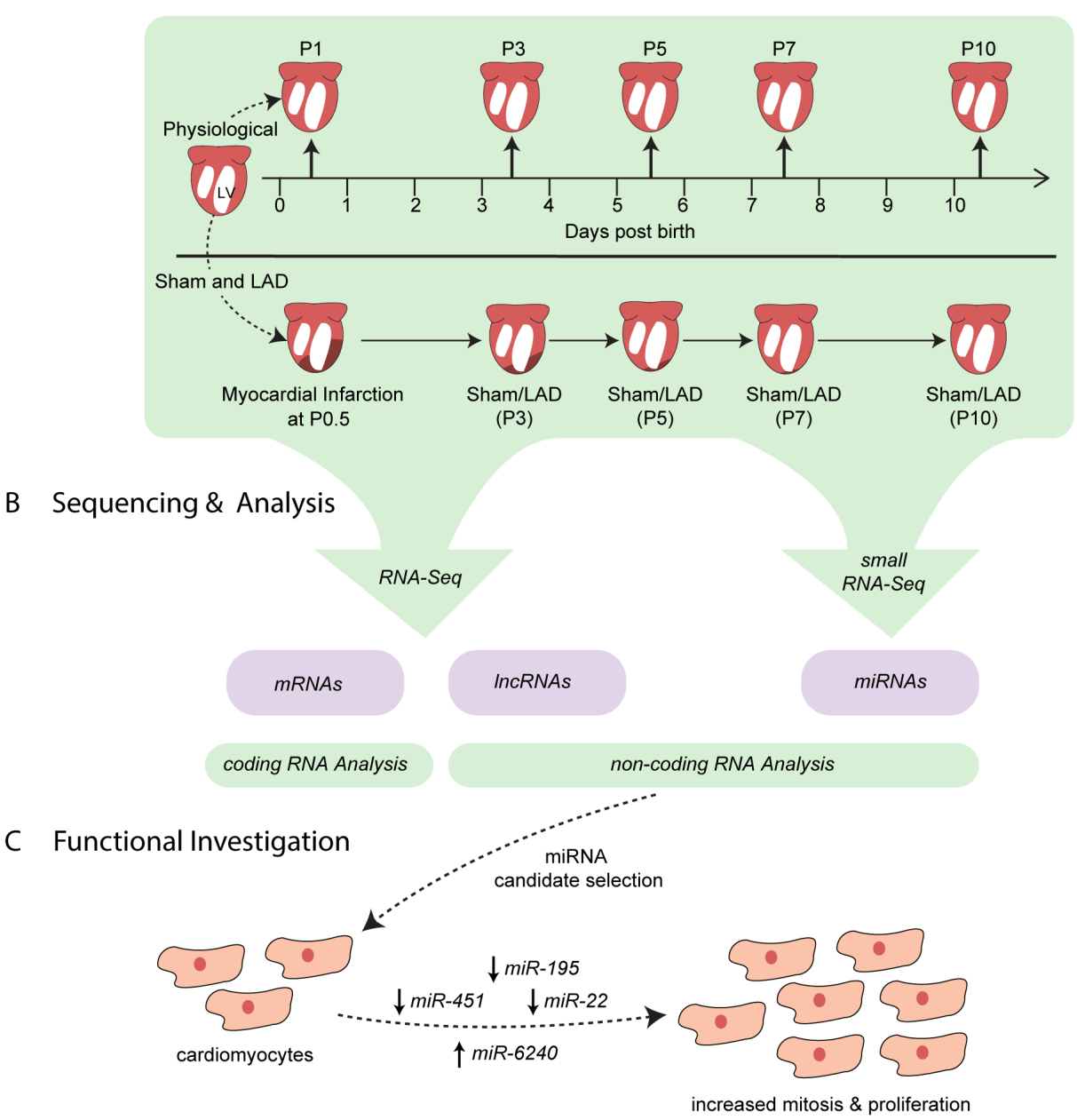

Figure 2. Changes of mRNA expression in physiological LV and following MI.

All mRNA sequencing experiments and data analyses were performed in individual animals for each time point and condition.

(A) KEGG pathway analysis between adjacent pairwise comparisons in physiological LV. (B) Venn diagram showing numbers of DE mRNAs between physiological pairwise comparison (C) Top 40 DE mRNAs between P5 and P7, (D) DE transcripts between LAD and sham samples-pairwise comparison, (E) KEGG pathway analysis between LAD and sham samples is pairwise comparison, (F) Top 40 DE mRNAs between LAD and sham 3 days post-surgery, (G) Overlap between DE coding transcripts in physiological and MI LVs.

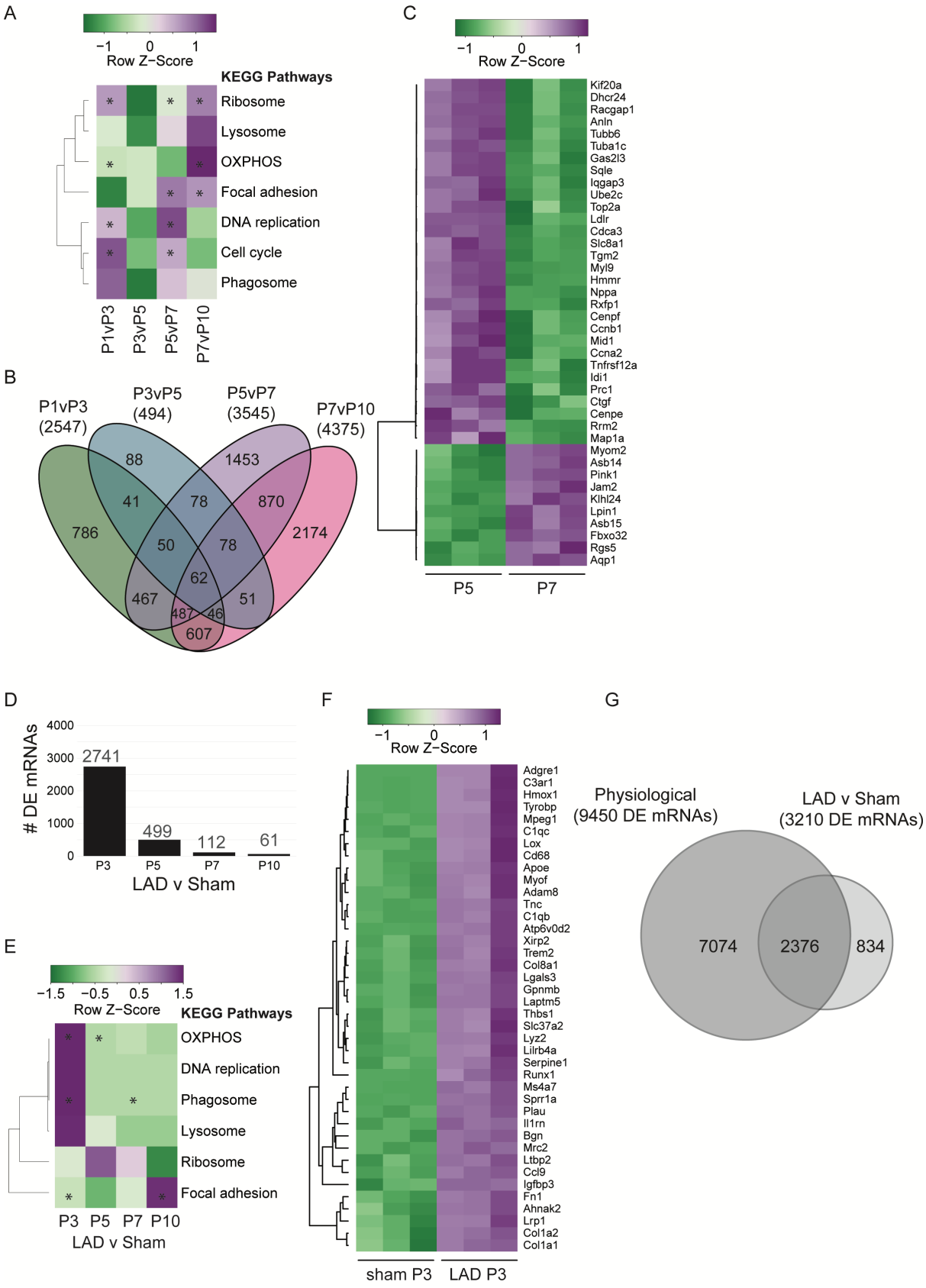
A
Row Z−Score
KEGG Pathways
Ribosome
Lysosome
OXPHOS
Focal adhesion
DNA replication
Cell cycle
Phagosome
P1vP3
P3vP5
P5vP7
P7vP10
B
P1vP3 (2547)
P3vP5 (494)
P5vP7 (3545)
P7vP10 (4375)
88
1453
41
78
870
786
50
78
2174
62
467
51
487
46
607
C
Row Z−Score
Kif20a
Dhcr24
Racgap1
Anln
Tubb6
Tuba1c
Gas2l3
Sqle
Iqgap3
Ube2c
Top2a
Ldlr
Cdca3
Slc8a1
Tgm2
Myl9
Hmmr
Nppa
Rxfp1
Cenpf
Ccnb1
Mid1
Ccna2
Tnfrsf12a
Idi1
Prc1
Ctgf
Cenpe
Rrm2
Map1a
Myom2
Asb14
Pink1
Jam2
Klhl24
Lpin1
Asb15
Fbxo32
Rgs5
Aqp1
P5
P7
D
DE mRNAs
2741
499
112
61
P3
P5
P7
P10
LAD v Sham
E
Row Z−Score
KEGG Pathways
OXPHOS
DNA replication
Phagosome
Lysosome
Ribosome
Focal adhesion
P3 P5 P7 P10
LAD v Sham
F
Row Z−Score
Adgre1
C3ar1
Hmox1
Tyrobp
Mpeg1
C1qc
Lox
Cd68
Apoe
Myof
Adam8
Tnc
C1qb
Atp6v0d2
Xirp2
Trem2
Col8a1
Lgals3
Gpnmb
Laptm5
Thbs1
Slc37a2
Lyz2
Lilrb4a
Serpine1
Runx1
Ms4a7
Sprr1a
Plau
Il1rn
Bgn
Mrc2
Ltbp2
Ccl9
Igfbp3
Fn1
Ahnak2
Lrp1
Col1a2
Col1a1
sham P3
LAD P3
G
Physiological (9450 DE mRNAs)
LAD v Sham (3210 DE mRNAs)
7074
2376
834

455

456

457

Figure 3. Changes of lncRNA expression in physiological LV and following MI.

All lncRNA sequencing experiments and data analyses were performed in individual animals for each time point and condition.

(A) Venn diagram showing numbers of DE lncRNAs between adjacent pairwise comparisons in physiological time points. (B) Top 40 most DE transcripts between P5 and P7. (C) The number of correlating DE mRNAs with DE lncRNAs in the increasing distance from transcription start site (TSS). (D) Numbers of DE lncRNAs following sham and LAD operations in pairwise comparisons. (E) Identities of the most DE lncRNAs between sham and LAD-operated LVs three days post-surgery. (F) Overlap between DE lncRNAs between physiological LVs and following surgery.

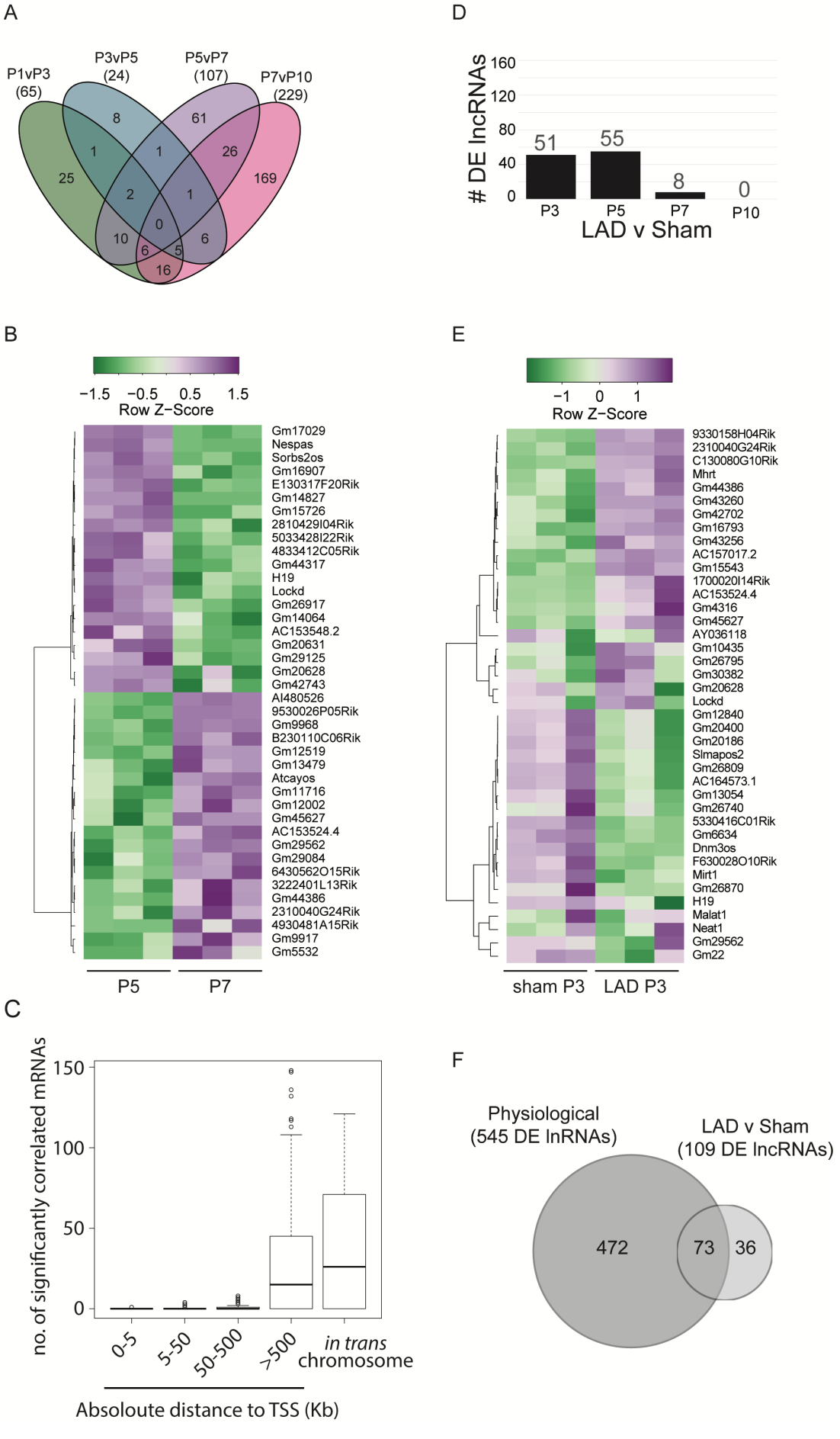
A
P1vP3
(65)
P3vP5
(24)
P5vP7
(107)
P7vP10
(229)
25
8
61
1
1
26
169
2
1
0
10
6
6
5
16
D
DE lncRNAs
160
120
80
40
0
51
55
8
0
P3
P5
P7
P10
LAD v Sham
B
−1.5 −0.5 0.5 1.5
Row Z−Score
Gm17029
Nespas
Sorbs2os
Gm16907
E130317F20Rik
Gm14827
Gm15726
2810429I04Rik
5033428I22Rik
4833412C05Rik
Gm44317
H19
Lockd
Gm26917
Gm14064
AC153548.2
Gm20631
Gm29125
Gm20628
Gm42743
AI480526
9530026P05Rik
Gm9968
B230110C06Rik
Gm12519
Gm13479
Atcayos
Gm11716
Gm12002
Gm45627
AC153524.4
Gm29562
Gm29084
6430562O15Rik
3222401L13Rik
Gm44386
2310040G24Rik
4930481A15Rik
Gm9917
Gm5532
P5
P7
E
−1 0 1
Row Z−Score
9330158H04Rik
2310040G24Rik
C130080G10Rik
Mhrt
Gm44386
Gm43260
Gm42702
Gm16793
Gm43256
AC157017.2
Gm15543
1700020I14Rik
AC153524.4
Gm4316
Gm45627
AY036118
Gm10435
Gm26795
Gm30382
Gm20628
Lockd
Gm12840
Gm20400
Gm20186
Slmapos2
Gm26809
AC164573.1
Gm13054
Gm26740
5330416C01Rik
Gm6634
Dnm3os
F630028O10Rik
Mirt1
Gm26870
H19
Malat1
Neat1
Gm29562
Gm22
sham P3
LAD P3
C
no. of significantly correlated mRNAs
150
100
50
0
0-5
5-50
50-500
>500
in trans
chromosome
Absoloute distance to TSS (Kb)
F
Physiological
(545 DE lnRNAs)
LAD v Sham
(109 DE lncRNAs)
472
73
36

468

Figure 4. Changes of miRNA expression in physiological LV and following MI.

All miRNA sequencing experiments and data analyses were performed in individual animals for each time point and condition.

(A) Venn diagram showing numbers of DE miRNAs between adjacent pairwise comparisons in physiological time points. (B) Heat map showing 40 most DE expressed miRNAs. (C) Focal adhesion and growth factor pathways diagram showing the genes targeted by DE miRNAs. (D) Numbers of DE miRNAs following MI. (E) Heat map of the most DE miRNAs three days post MI. (F) Overlap between DE miRNAs between physiological LVs and following surgery.

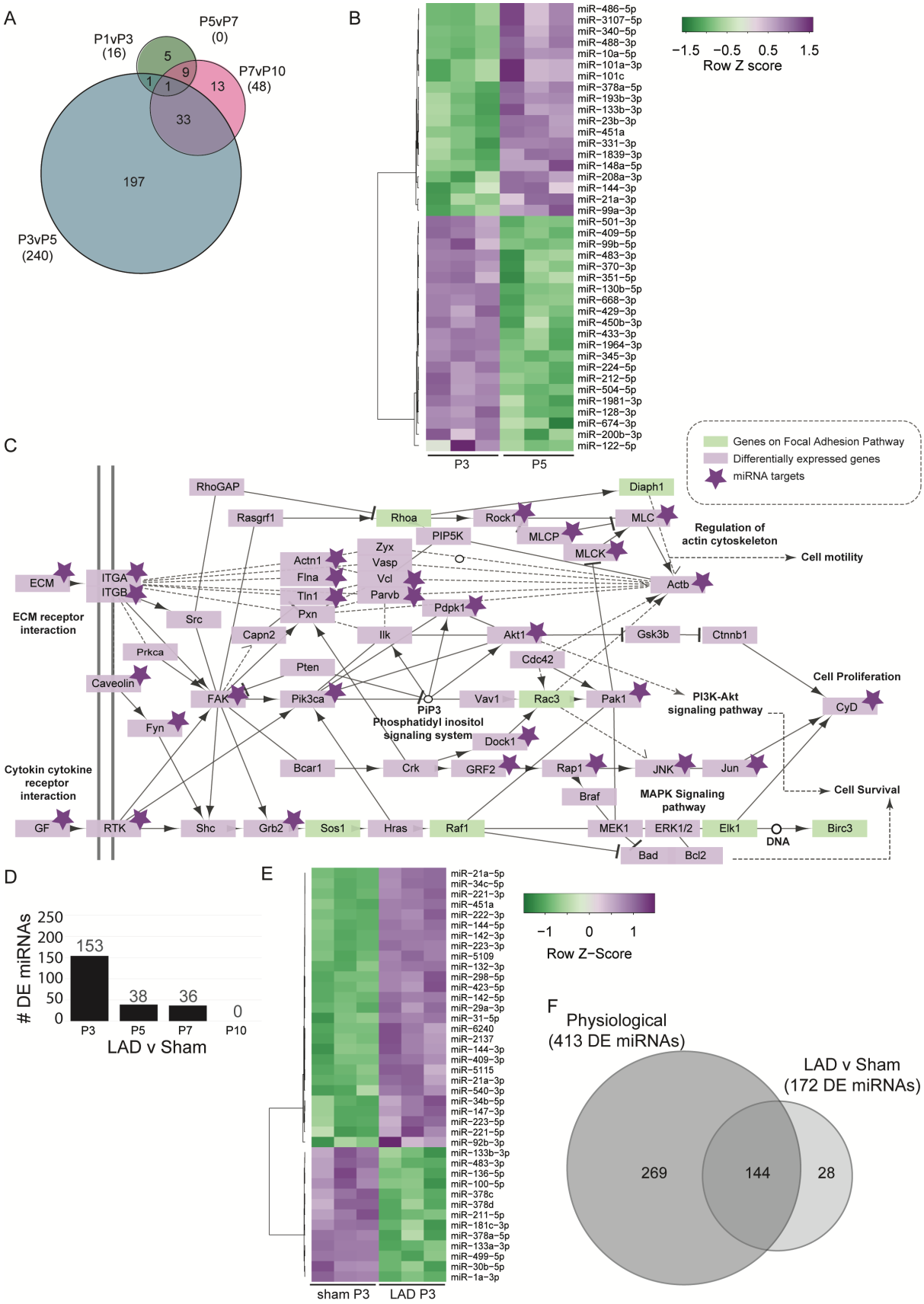
A
P1vP3
(16)
P5vP7
(0)
P7vP10
(48)
P3vP5
(240)
5
9
1
1
13
33
197
B
miR−486−5p
miR−3107−5p
miR−340−5p
miR−488−3p
miR−10a−5p
miR−101a−3p
miR−101c
miR−378a−5p
miR−193b−3p
miR−133b−3p
miR−23b−3p
miR−451a
miR−331−3p
miR−1839−3p
miR−148a−5p
miR−208a−3p
miR−144−3p
miR−21a−3p
miR−99a−3p
miR−501−3p
miR−409−5p
miR−99b−5p
miR−483−3p
miR−370−3p
miR−351−5p
miR−130b−5p
miR−668−3p
miR−429−3p
miR−450b−3p
miR−433−3p
miR−1964−3p
miR−345−3p
miR−224−5p
miR−212−5p
miR−504−5p
miR−1981−3p
miR−128−3p
miR−674−3p
miR−200b−3p
miR−122−5p
P3
P5
−1.5 −0.5 0.5 1.5
Row Z score
C
Genes on Focal Adhesion Pathway
Differentially expressed genes
miRNA targets
RhoGAP
Rasgrf1
Rhoa
Rock1
Diaph1
MLC
MLCP
MLCK
PIP5K
Regulation of
actin cytoskeleton
Cell motility
Actn1
Flna
Tln1
Pxn
Zyx
Vasp
Vcl
Parvb
Actb
ECM
ITGA
ITGB
ECM receptor
interaction
Src
Pdpk1
Capn2
Ilk
Akt1
Gsk3b
Ctnnb1
Prkca
Cdc42
Pten
Caveolin
FAK
Pik3ca
PiP3
Phosphatidyl inositol
signaling system
Vav1
Rac3
Pak1
PI3K-Akt
signaling pathway
Cell Proliferation
CyD
Fyn
Dock1
Bcar1
Crk
GRF2
Rap1
JNK
Jun
Cytokin cytokine
receptor
interaction
Braf
MAPK Signaling
pathway
Cell Survival
GF
RTK
Shc
Grb2
Sos1
Hras
Raf1
MEK1
ERK1/2
Elk1
DNA
Birc3
Bad
Bcl2
D
DE miRNAs
250
200
150
100
50
0
153
38
36
0
P3
P5
P7
P10
LAD v Sham
E
miR−21a−5p
miR−34c−5p
miR−221−3p
miR−451a
miR−222−3p
miR−144−5p
miR−142−3p
miR−223−3p
miR−5109
miR−132−3p
miR−298−5p
miR−423−5p
miR−142−5p
miR−29a−3p
miR−31−5p
miR−6240
miR−2137
miR−144−3p
miR−409−3p
miR−5115
miR−21a−3p
miR−540−3p
miR−34b−5p
miR−147−3p
miR−223−5p
miR−221−5p
miR−92b−3p
miR−133b−3p
miR−483−3p
miR−136−5p
miR−100−5p
miR−378c
miR−378d
miR−211−5p
miR−181c−3p
miR−378a−5p
miR−133a−3p
miR−499−5p
miR−30b−5p
miR−1a−3p
sham P3
LAD P3
−1 0 1
Row Z−Score
F
Physiological
(413 DE miRNAs)
LAD v Sham
(172 DE miRNAs)
269
144
28

477

478

Figure 5. Functional analysis of miR inhibition and overexpression in P5 mouse and human cardiomyocytes.

Functional analysis experiments were performed in triplicates for each cell type and each transfection miRNA.

(A) Changes in mRNA expression of cell cycle regulating cyclins in P5 mouse primary cardiomyocytes following treatment with miRNA inhibitors and mimic. A significance indicated by star. EdU and pH3 staining revealing number of proliferating (B) and dividing cells (C) following treatment with miRNAs. (D) Changes in mRNA expression of cell cycle regulating cyclins in human iPSC derived cardiomyocytes following treatment with miRNA inhibitors and mimic. EdU and pH3 staining revealing number of proliferating (E) and dividing cells (F) iPSC derived cardiomyocytes following treatment with miRNAs.

A significance vs. scramble control indicated by stars as follows: *** $p \leq 0.001$, ** $p \leq 0.01$, * $p \leq 0.05$.

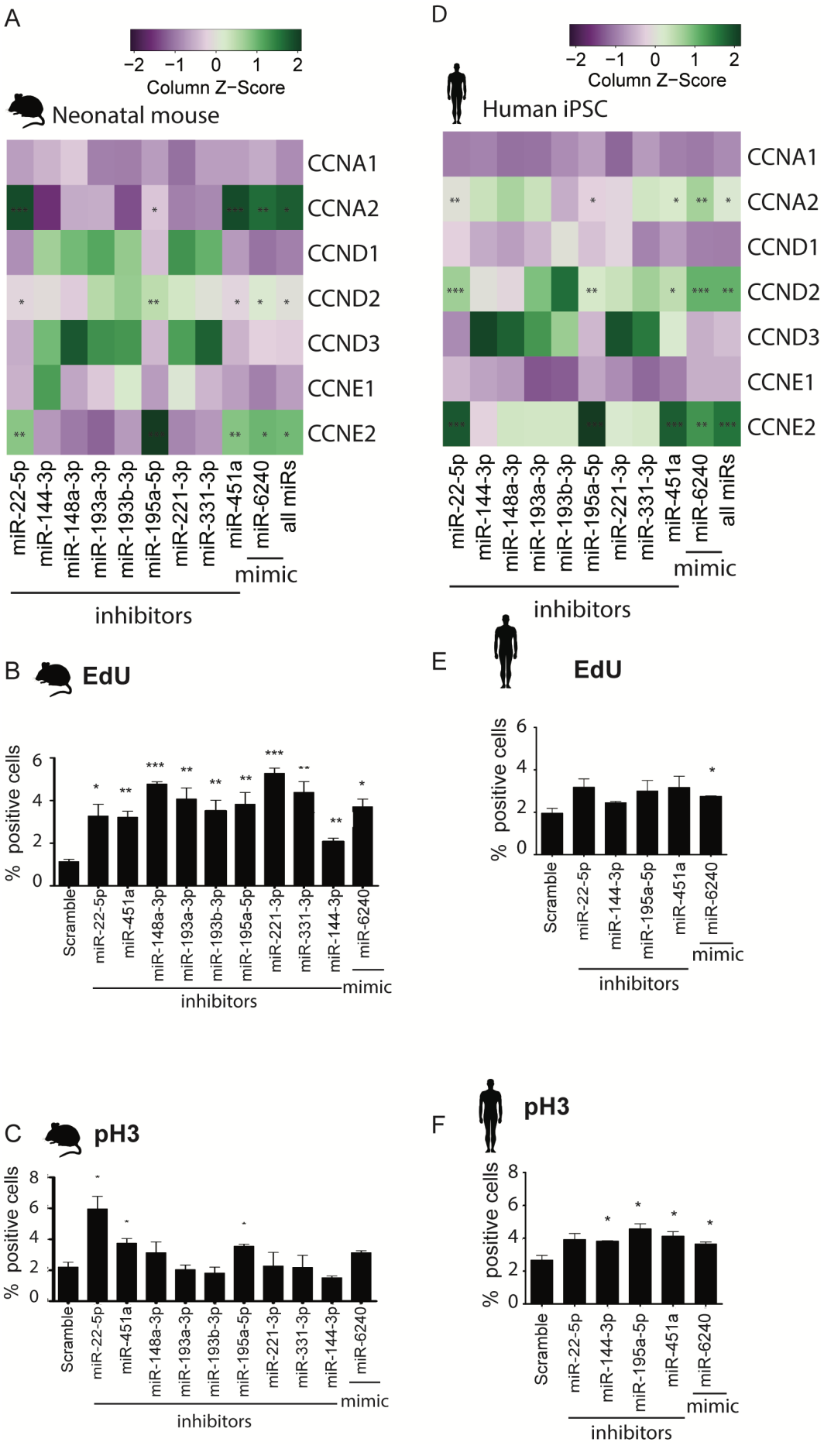
A
−2 −1 0 1 2
Column Z−Score
Neonatal mouse
CCNA1
CCNA2
CCND1
CCND2
CCND3
CCNE1
CCNE2
miR-22-5p
miR-144-3p
miR-148a-3p
miR-193a-3p
miR-193b-3p
miR-195a-5p
miR-221-3p
miR-331-3p
miR-451a
miR-6240
all miRs
mimic
inhibitors
D
−2 −1 0 1 2
Column Z−Score
Human iPSC
CCNA1
CCNA2
CCND1
CCND2
CCND3
CCNE1
CCNE2
miR-22-5p
miR-144-3p
miR-148a-3p
miR-193a-3p
miR-193b-3p
miR-195a-5p
miR-221-3p
miR-331-3p
miR-451a
miR-6240
all miRs
mimic
inhibitors
B
EdU
% positive cells
Scramble
miR-22-5p
miR-451a
miR-148a-3p
miR-193a-3p
miR-193b-3p
miR-195a-5p
miR-221-3p
miR-331-3p
miR-144-3p
miR-6240
mimic
inhibitors
E
EdU
% positive cells
Scramble
miR-22-5p
miR-144-3p
miR-195a-5p
miR-451a
miR-6240
mimic
inhibitors
C
pH3
% positive cells
Scramble
miR-22-5p
miR-451a
miR-148a-3p
miR-193a-3p
miR-193b-3p
miR-195a-5p
miR-221-3p
miR-331-3p
miR-144-3p
miR-6240
mimic
inhibitors
F
pH3
% positive cells
Scramble
miR-22-5p
miR-144-3p
miR-195a-5p
miR-451a
miR-6240
mimic
inhibitors

492

References

1. Moran AE, Forouzanfar MH, Roth GA, Mensah GA, Ezzati M, Murray CJ, et al. Temporal trends in ischemic heart disease mortality in 21 world regions, 1980 to 2010: the Global Burden of Disease 2010 study. *Circulation*. 2014;129:1483-1492.
2. Schnapp E, Kragl M, Rubin L and Tanaka EM. Hedgehog signaling controls dorsoventral patterning, blastema cell proliferation and cartilage induction during axolotl tail regeneration. *Development*. 2005;132:3243-3253.
3. Nacu E and Tanaka EM. Limb regeneration: a new development? *Annu Rev Cell Dev Biol*. 2011;27:409-440.
4. Mahmoud AI, O'Meara CC, Gemberling M, Zhao L, Bryant DM, Zheng R, et al. Nerves Regulate Cardiomyocyte Proliferation and Heart Regeneration. *Dev Cell*. 2015;34:387-399.
5. Wagers AJ and Conboy IM. Cellular and molecular signatures of muscle regeneration: current concepts and controversies in adult myogenesis. *Cell*. 2005;122:659-667.
6. Seifert AW, Kiama SG, Seifert MG, Goheen JR, Palmer TM and Maden M. Skin shedding and tissue regeneration in African spiny mice (Acomys). *Nature*. 2012;489:561-565.
7. Jugdutt BI, Joljart MJ and Khan MI. Rate of collagen deposition during healing and ventricular remodeling after myocardial infarction in rat and dog models. *Circulation*. 1996;94:94-101.
8. Lutgens E, Daemen MJ, de Muinck ED, Debets J, Leenders P and Smits JF. Chronic myocardial infarction in the mouse: cardiac structural and functional changes. *Cardiovasc Res*. 1999;41:586-593.
9. Naqvi N, Li M, Calvert JW, Tejada T, Lambert JP, Wu J, et al. A proliferative burst during preadolescence establishes the final cardiomyocyte number. *Cell*. 2014;157:795-807.
10. Alkass K, Panula J, Westman M, Wu TD, Guerquin-Kern JL and Bergmann O. No Evidence for Cardiomyocyte Number Expansion in Preadolescent Mice. *Cell*. 2015;163:1026-1036.
11. Li F, Wang X, Capasso JM and Gerdes AM. Rapid transition of cardiac myocytes from hyperplasia to hypertrophy during postnatal development. *J Mol Cell Cardiol*. 1996;28:1737-1746.
12. Soonpaa MH, Kim KK, Pajak L, Franklin M and Field LJ. Cardiomyocyte DNA synthesis and binucleation during murine development. *Am J Physiol*. 1996;271:H2183-2189.
13. Puente BN, Kimura W, Muralidhar SA, Moon J, Amatruda JF, Phelps KL, et al. The oxygen-rich postnatal environment induces cardiomyocyte cell-cycle arrest through DNA damage response. *Cell*. 2014;157:565-579.
14. Porrello ER, Mahmoud AI, Simpson E, Hill JA, Richardson JA, Olson EN, et al. Transient regenerative potential of the neonatal mouse heart. *Science*. 2011;331:1078-1080.
15. Haubner BJ, Adamowicz-Brice M, Khadayate S, Tiefenthaler V, Metzler B, Aitman T, et al. Complete cardiac regeneration in a mouse model of myocardial infarction. *Aging (Albany NY)*. 2012;4:966-977.
16. Porrello ER, Mahmoud AI, Simpson E, Johnson BA, Grinsfelder D, Canseco D, et al. Regulation of neonatal and adult mammalian heart regeneration by the miR-15 family. *Proc Natl Acad Sci U S A*. 2013;110:187-192.
17. Tanaka EM and Reddien PW. The cellular basis for animal regeneration. *Dev Cell*. 2011;21:172-185.
18. Sikes JM and Newmark PA. Restoration of anterior regeneration in a planarian with limited regenerative ability. *Nature*. 2013;500:77-80.
19. Rodius S, Androsova G, Gotz L, Liechti R, Crespo I, Merz S, et al. Analysis of the dynamic co-expression network of heart regeneration in the zebrafish. *Sci Rep*. 2016;6:26822.
20. Porrello ER, Johnson BA, Aurora AB, Simpson E, Nam YJ, Matkovich SJ, et al. MiR-15 family regulates postnatal mitotic arrest of cardiomyocytes. *Circ Res*. 2011;109:670-679.
21. Aguirre A, Montserrat N, Zacchigna S, Nivet E, Hishida T, Krause MN, et al. In vivo activation of a conserved microRNA program induces mammalian heart regeneration. *Cell Stem Cell*. 2014;15:589-604.

22. Grote P, Wittler L, Hendrix D, Koch F, Wahrisch S, Beisaw A, et al. The tissue-specific lncRNA Fendrr is an essential regulator of heart and body wall development in the mouse. *Dev Cell*. 2013;24:206-214.
23. Klattenhoff CA, Scheuermann JC, Surface LE, Bradley RK, Fields PA, Steinhauser ML, et al. Braveheart, a long noncoding RNA required for cardiovascular lineage commitment. *Cell*. 2013;152:570-583.
24. Han P, Li W, Lin CH, Yang J, Shang C, Nurnberg ST, et al. A long noncoding RNA protects the heart from pathological hypertrophy. *Nature*. 2014;514:102-106.
25. Wang K, Liu CY, Zhou LY, Wang JX, Wang M, Zhao B, et al. APF lncRNA regulates autophagy and myocardial infarction by targeting miR-188-3p. *Nat Commun*. 2015;6:6779.
26. Viereck J, Kumarswamy R, Foinquinos A, Xiao K, Avramopoulos P, Kunz M, et al. Long noncoding RNA Chast promotes cardiac remodeling. *Sci Transl Med*. 2016;8:326ra322.
27. O'Meara CC, Wamstad JA, Gladstone RA, Fomovsky GM, Butty VL, Shrikumar A, et al. Transcriptional reversion of cardiac myocyte fate during mammalian cardiac regeneration. *Circ Res*. 2015;116:804-815.
28. Patro R, Duggal G, Love MI, Irizarry RA and Kingsford C. Salmon provides fast and bias-aware quantification of transcript expression. *Nat Methods*. 2017;14:417-419.
29. Goldmann WH. Mechanotransduction and focal adhesions. *Cell Biol Int*. 2012;36:649-652.
30. Barr FA and Gruneberg U. Cytokinesis: placing and making the final cut. *Cell*. 2007;131:847-860.
31. Kabeche L and Compton DA. Cyclin A regulates kinetochore microtubules to promote faithful chromosome segregation. *Nature*. 2013;502:110-113.
32. Pennock E, Buckley K and Lundblad V. Cdc13 delivers separate complexes to the telomere for end protection and replication. *Cell*. 2001;104:387-396.
33. Toledo CM, Herman JA, Olsen JB, Ding Y, Corrin P, Girard EJ, et al. BuGZ is required for Bub3 stability, Bub1 kinetochore function, and chromosome alignment. *Dev Cell*. 2014;28:282-294.
34. Banerjee I, Fuseler JW, Price RL, Borg TK and Baudino TA. Determination of cell types and numbers during cardiac development in the neonatal and adult rat and mouse. *Am J Physiol Heart Circ Physiol*. 2007;293:H1883-1891.
35. Matsuoka K, Asano Y, Higo S, Tsukamoto O, Yan Y, Yamazaki S, et al. Noninvasive and quantitative live imaging reveals a potential stress-responsive enhancer in the failing heart. *FASEB J*. 2014;28:1870-1879.
36. Aurora AB, Porrello ER, Tan W, Mahmoud AI, Hill JA, Bassel-Duby R, et al. Macrophages are required for neonatal heart regeneration. *J Clin Invest*. 2014;124:1382-1392.
37. Godwin JW, Pinto AR and Rosenthal NA. Macrophages are required for adult salamander limb regeneration. *Proc Natl Acad Sci U S A*. 2013;110:9415-9420.
38. Hao Y, Crenshaw T, Moulton T, Newcomb E and Tycko B. Tumour-suppressor activity of H19 RNA. *Nature*. 1993;365:764-767.
39. Keniry A, Oxley D, Monnier P, Kyba M, Dandolo L, Smits G, et al. The H19 lincRNA is a developmental reservoir of miR-675 that suppresses growth and Igf1r. *Nat Cell Biol*. 2012;14:659-665.
40. Yang F, Bi J, Xue X, Zheng L, Zhi K, Hua J, et al. Up-regulated long non-coding RNA H19 contributes to proliferation of gastric cancer cells. *FEBS J*. 2012;279:3159-3165.
41. Barlow DP and Bartolomei MS. Genomic imprinting in mammals. *Cold Spring Harb Perspect Biol*. 2014;6.
42. Menheniott TR, Woodfine K, Schulz R, Wood AJ, Monk D, Giraud AS, et al. Genomic imprinting of Dopa decarboxylase in heart and reciprocal allelic expression with neighboring Grb10. *Mol Cell Biol*. 2008;28:386-396.
43. Balaban NQ, Schwarz US, Riveline D, Goichberg P, Tzur G, Sabanay I, et al. Force and focal adhesion assembly: a close relationship studied using elastic micropatterned substrates. *Nat Cell Biol*. 2001;3:466-472.
44. Ross RS and Borg TK. Integrins and the myocardium. *Circ Res*. 2001;88:1112-1119.

45. Roovers K and Assoian RK. Effects of rho kinase and actin stress fibers on sustained extracellular signal-regulated kinase activity and activation of G(1) phase cyclin-dependent kinases. *Mol Cell Biol*. 2003;23:4283-4294.
46. Huang ZP and Wang DZ. miR-22 in cardiac remodeling and disease. *Trends Cardiovasc Med*. 2014;24:267-272.
47. Nunes Bastos R, Gandhi SR, Baron RD, Gruneberg U, Nigg EA and Barr FA. Aurora B suppresses microtubule dynamics and limits central spindle size by locally activating KIF4A. *J Cell Biol*. 2013;202:605-621.
48. Chen L, Fulcoli FG, Tang S and Baldini A. Tbx1 regulates proliferation and differentiation of multipotent heart progenitors. *Circ Res*. 2009;105:842-851.
49. David JJ, Subramanian SV, Zhang A, Willis WL, Kelm RJ, Jr., Leier CV, et al. Y-box binding protein-1 implicated in translational control of fetal myocardial gene expression after cardiac transplant. *Exp Biol Med (Maywood)*. 2012;237:593-607.
50. Yang KC, Ku YC, Lovett M and Nerbonne JM. Combined deep microRNA and mRNA sequencing identifies protective transcriptomal signature of enhanced PI3Kalpha signaling in cardiac hypertrophy. *J Mol Cell Cardiol*. 2012;53:101-112.
51. Uosaki H, Cahan P, Lee DI, Wang S, Miyamoto M, Fernandez L, et al. Transcriptional Landscape of Cardiomyocyte Maturation. *Cell Rep*. 2015;13:1705-1716.
52. Yin VP, Lepilina A, Smith A and Poss KD. Regulation of zebrafish heart regeneration by miR-133. *Dev Biol*. 2012;365:319-327.
53. Beauchemin M, Smith A and Yin VP. Dynamic microRNA-101a and Fosab expression controls zebrafish heart regeneration. *Development*. 2015;142:4026-4037.
54. Gan J, Sonntag HJ, Tang MK, Cai D and Lee KK. Integrative Analysis of the Developing Postnatal Mouse Heart Transcriptome. *PLoS One*. 2015;10:e0133288.
55. Eulalio A, Mano M, Dal Ferro M, Zentilin L, Sinagra G, Zacchigna S, et al. Functional screening identifies miRNAs inducing cardiac regeneration. *Nature*. 2012;492:376-381.